

Imaging and spectroscopy of arcs around the most luminous X-ray cluster RX J1347.5-1145¹

Kailash C. Sahu², Richard A. Shaw², Mary Elizabeth Kaiser^{3 6}, Stefi A. Baum², Henry C. Ferguson², Jeffrey J. E. Hayes², Theodore R. Gull³, Robert J. Hill⁴, John B. Hutchings⁵, Randy A. Kimble³, Philip Plait⁷, Bruce E. Woodgate³

ABSTRACT

The cluster RX J1347.5-1145, the most luminous cluster in the X-ray wavelengths, was imaged with the newly installed Space Telescope Imaging Spectrograph (STIS) on-board HST. Its relatively high redshift (0.451) and luminosity indicate that this is one of the most massive of all known clusters. The STIS images unambiguously show several arcs in the cluster. The largest two arcs ($>5''$ length) are symmetrically situated on opposite sides of the cluster, at a distance of ~ 35 arcsec from the central galaxy. The STIS images also show approximately 100 faint galaxies within the radius of the arcs whose combined luminosity is $\sim 4 \times 10^{11} L_{\odot}$. We also present ground-based spectroscopic observations of the northern arc which show one clear emission line at $\sim 6730 \text{ \AA}$, which is consistent with an identification as [OII] 3727 \AA , implying a redshift of 0.81 for this arc. The southern arc shows a faint continuum but no emission features. The surface mass within the radius of the arcs (240 kpc), as derived from the gravitational lensing, is $\sim 6.3 \times 10^{14} M_{\odot}$. The resultant mass-to-light ratio of ~ 1200 is higher than what is seen in many clusters but smaller than the value recently derived for some ‘dark’ X-ray clusters (Hattori et al. 1997). The total surface mass derived from the X-ray flux within the radius of the arcs is $\sim 2.1 - 6.8 \times 10^{14} M_{\odot}$, which implies that the ratio of the gravitational to the X-ray mass is ~ 1 to 3 . The surface *gas* mass within this radius is $\sim 3.5 \times 10^{13} M_{\odot}$, which implies that at least 6% of the total mass within this region is baryonic.

¹Based on observations with the NASA/ESA *Hubble Space Telescope*, obtained at the Space Telescope Science Institute, which is operated by AURA Inc under NASA contract NAS5-26555, and the 3.6-meter telescope of the European Southern Observatory at La Silla, Chile.

²Space Telescope Science Institute, 3700 San Martin Drive, Baltimore, MD 21218

³NASA/Goddard Space Flight Center, Code 681, Greenbelt, MD 20771

⁴Hughes/STX Corporation NASA/Goddard Space Flight Center, Code 681, Greenbelt, MD 20771

⁵Dominion Astrophysical Observatory, National Research Council of Canada, 5071 Saanich Rd., Victoria, B.C. V8X 4M6, Canada

⁶Dept of Physics and Astronomy, Johns Hopkins University, Baltimore, MD 21218

⁷Advanced Computer Concepts, NASA/GSFC, Code 681, Greenbelt, MD 20771

1. Introduction

Clusters of galaxies are the most massive gravitationally bound systems in the Universe. They serve as important probes of the large-scale structures and their evolution (see e.g. Bahcall, 1988). Accurate mass determination of such clusters can place very useful constraints on Ω and the nature of the dark matter (White and Fabian, 1995).

RXJ 1347.5-1145 (RA(2000) = $13^h 47^m 30.^s5$ Dec(2000) = $-11^\circ 45' 09''$) is the most luminous X-ray cluster among all the clusters observed in the ROSAT all sky survey (Schindler et al. 1995). Its high luminosity coupled with a redshift of 0.451 implies that this is one of the most massive of all clusters known to date.

The cluster has two optically bright galaxies at the center. Optical spectra for these brightest cluster members indicate that the cluster is at a redshift of $z=0.451$ (Schindler et al., 1995). Optical images obtained by Schindler et al. (1995) and Fischer and Tyson (1997) show two possible bright arcs symmetrically situated at ~ 35 arcsec away from the brightest cluster member and some hint of other arcs, requiring higher spatial resolution images for confirmation. Spectral observations for the arcs were not available. This paper presents high spatial-resolution images obtained with STIS, and ground-based spectroscopic observations for the arc, which are used to estimate the mass of the cluster.

2. Mass-distribution from X-ray observations

Many of the X-ray bright clusters show the presence of gravitationally lensed arcs. From an optical follow-up study of 41 X-ray bright clusters, Gioia and Luppino (1994) showed that compared to an optically selected sample, the X-ray selected sample has 3 times larger probability of showing gravitationally lensed arcs. This clearly indicates that the luminous X-ray clusters are massive, perhaps the most massive of all observed objects in the universe. Their total mass determination is clearly important, and their mass profile may give important clues to the nature of the dark matter.

These X-ray clusters provide an opportunity not only to study these most massive members of the universe, but also to study the properties of background galaxies imaged as arcs. The gravitational lensing facilitates this study in two important ways. First, it provides a direct way to derive the mass of the lensing cluster. Secondly, it increases the brightness of the background galaxy by the formation of the arcs, thereby enabling us to study the background galaxy which would have otherwise been too faint to be studied.

In the ROSAT band of 0.1 to 2.4 keV, the X-ray emission from RXJ1347.5-1145 extends to a radius of ~ 4.2 arcmin, with an observed luminosity of 7.3×10^{45} erg s $^{-1}$ within this radius. The ASCA observations (2 - 10 keV) show emission out to a radius of ~ 6.4 arcmin, with an observed luminosity of 4.6×10^{45} erg s $^{-1}$ in this band. From the X-ray observations the mass distributions

within radii of 240 kpc, 1 Mpc, and 3 Mpc have been derived. The total surface mass within the radius of the large arcs (240 kpc) is $2.1 \times 10^{14} M_{\odot}$ (Schindler et al. 1997) to $6.8 \times 10^{14} M_{\odot}$ (Allen, 1997). Within a radius of 1 Mpc, the gas mass is $2.0 \times 10^{14} M_{\odot}$ and the total mass, assuming hydrostatic equilibrium, is $5.8 \times 10^{14} M_{\odot}$. On the 3 Mpc scale, the gas mass is $8.9 \times 10^{14} M_{\odot}$ and the total mass is $1.7 \times 10^{15} M_{\odot}$.

3. Observations

The newly installed Space Telescope Imaging Spectrograph (STIS) on board HST was used to get the images of RX J1347.5-1145. Observations were taken on 25 May 1997, with the CCD detector using the clear and the long-pass filtered apertures (Baum et al. 1996). A mosaic of 4 ($50'' \times 50''$) unfiltered CCD images was taken to encompass the field of arcs which span $>70''$. The field of view of the long pass filter ($28'' \times 50''$) is smaller than the clear aperture. As a consequence, only the brightest central galaxy and arc 2 were imaged with this filter. The integration times for each telescope pointing ranged from 250 to 300 seconds.

Spectroscopic observations were taken using the versatile, high-throughput EFOSC (ESO Faint Object Spectrographic Camera) at the ESO 3.6m telescope at La Silla, Chile. The camera has both imaging and spectroscopic capabilities. Since the spectrograph can hold 5 gratings simultaneously, multiple spectral resolutions and bandpasses were easily configured. A log of the spectroscopic observations is provided in Table 1.

First, a direct image of the field was obtained with an exposure of 30 sec. The seeing at this time was $\sim 1.5''$. A field of view of $5.2' \times 5.2'$ was obtained using the 512×512 pixel Tektronix CCD. A slit of $1.5''$ width was used for all the observations. The first spectra were obtained with the R300 grating, with the slit oriented so that the northern arc was along the length of the slit. A single, bright emission feature at $\sim 6730 \text{ \AA}$ with a faint continuum on either side can be seen in each of the two exposures taken in this configuration. Spectra obtained in the blue with the B300 grating did not show any additional features. The two galaxies were placed in the slit and 3 exposures, each of 20 minutes duration, were taken with R300 grating. Fig. 1 shows the combined spectrum for the northern arc and the two central galaxies.

Similar observations were taken for the southern arc. Exposures of the southern arc in the same grating setup (R300) however showed no trace of emission; only a faint continuum was visible. Spectra were then taken with the B300 grating spanning the wavelength region from 3600 \AA to 6800 \AA . No features, except a faint continuum in the blue, are visible despite the fact that the detection limit for the southern arc is better than for the northern arc. If the arc has [OII] emission at 3727 \AA , then the observations indicate that it is redshifted beyond $\sim 7500 \text{ \AA}$ and into a region where numerous atmospheric absorption lines make detection difficult. This would indicate that the redshift is higher than 1. However, this object could also be a galaxy without any strong emission features in which case the continuum of the galaxy is consistent with a redshift on the

order of 0.8 to 1.5.

4. Data reduction and results

The STIS images were analyzed using both the STScI CALSTIS and the IDT CALSTIS calibration pipelines (both of which essentially employ the same procedure as mentioned above), and consistent results were obtained. The overscan regions were first subtracted from the raw CCD images. Two readouts per HST telescope pointing position were employed to facilitate cosmic ray rejection. The cosmic rays were removed using an algorithm which compares the two images and iteratively replaces pixels which deviate by more than 8σ with an appropriately weighted minimum value of the pixel. Next a bias image and a dark frame are subtracted from the data. This image is then flat fielded using a ground based calibration flat. The resulting image is then compared to the pipeline resident hot pixel table ($>0.1 \text{ count sec}^{-1} \text{ pixel}^{-1}$). Any residual hot pixels are then eliminated by visual inspection using a nearest neighbor interpolation algorithm.

A mosaic image was created by aligning the brightest feature in each of the overlap regions. The images were combined using the IRAF task ‘imcombine’, with a weighted average proportional to the exposure time for the overlapping regions, and counts normalized to a mean exposure time in the entire mosaic image. Fig. 2 (Plate 1) shows the resultant mosaic image. The image shows several arcs which are marked in the figure. The two large arcs (1 and 4), situated on opposite sides of the central galaxy are separated by about 70 arcsec; this is one of the largest separations seen in any cluster. Positional and dimensional information regarding the various arcs is given in Table 2.

The two large arcs were already seen from ground-based observations. However, due to the lower spatial resolution of the ground-based observations, the possibility that the arcs are foreground galaxies could not be ruled out (Fischer and Tyson, 1997). STIS observations unambiguously prove that these are arcs with magnifications (which, to a first order, is the length to width ratio) ranging from 7 to 15. There are 3 additional features whose orientation and distance from the center are consistent with being arcs, although the possibility that these smaller arcs may be foreground galaxies cannot be eliminated.

The two central galaxies are clearly resolved. Fig. 3 (Plate 2) shows an enlarged view of the central galaxy, which shows a clear jet-like structure on one side, and a similar but much fainter structure on the opposite side. These structures, which may be jets or tidal tails, are about $0.6''$ long, which corresponds to a length of $\sim 3 \text{ kpc}$. The FHHM of the central and the fainter galaxies, as derived from the average Moffat and Gaussian fit to their structure in different position angles, is 0.6 and 0.4 arcsec, respectively. The FWHM of the point sources in the field is $\sim 0.085 \text{ arcsec}$. Derived magnitudes for the two galaxies and the arcs are given in Table 3, which are consistent with those of Fischer and Tyson (1997).

The image processing software packages MIDAS and IRAF were used to reduce the spectral

data obtained from the ground. After bias subtraction, the frames were flat-field corrected with an average of 5 flat-field images taken with the dome illuminated with a tungsten lamp. The sky was taken from both sides of the spectrum for a good sky subtraction. The resulting one dimensional spectrum was then wavelength and flux calibrated. A He-Argon spectral lamp was used for wavelength calibration. For flux calibration the standard stars HD 8879, a fast rotating Be star, and LTT 9239 were used. In the wavelength region redward of 7500 Å there are several atmospheric emission lines, making it difficult to differentiate between these emission features and the source in this region. The resulting final spectra for the northern arc and the two galaxies are shown in Fig. 1.

5. Redshifts

5.1. The central galaxies

The spectra for the two central galaxies (Fig. 1) are consistent with the lower resolution (15 Å) spectra published by Schindler et al. (1995). Compared to the eastern galaxy, the central galaxy is brighter by ~ 0.4 magnitudes and is also bluer. The central galaxy shows emission features of $H\beta$ $\lambda 4861\text{\AA}$, and $[\text{OIII}]$ $\lambda 4959$ and 5007\AA , and the eastern galaxy shows a few absorption features, all of which indicate the lensing cluster to be at $z \sim 0.451$. Our higher resolution spectra also enable us to derive a velocity dispersion of 620 km s^{-1} for the central galaxy. Using the radius of the galaxy and the velocity dispersion, we derive (Binney and Tremaine, 1987) a mass of $2.4 \times 10^{11} M_{\odot}$ for the galaxy. However, this mass determination is valid only if the radius of the line emitting region is the same as the observed radius of the galaxy, and if the system is virialized. If the line emitting region is confined to a smaller region, this mass determination is not applicable. The mass of the line emitting region itself would be lower, but depending on the contribution of mass outside the line emitting region, the total mass can be higher or lower.

5.2. The arcs

Since the redshift of the lensing cluster is 0.45, the redshift of the arcs must be higher. This implies that the rest wavelength of the northern arc's emission line seen at 6730\AA is less than 4638\AA . This eliminates the possibility that the emission line could be either of the $H\beta$ $\lambda 4861\text{\AA}$, $[\text{OIII}]$ $\lambda 4959$ and 5007\AA or the $H\alpha$ $\lambda 6563 \text{\AA}$ lines. The only strong emission lines which may be responsible are the $[\text{OII}]$ $\lambda 3727 \text{\AA}$, CIV $\lambda 1550 \text{\AA}$ and $\text{Ly H}\alpha$ $\lambda 1216 \text{\AA}$ lines, with corresponding redshifts of 0.8, 3.34 and 4.53, respectively. Although we cannot rule out the possibility that the emission line could be either $\text{Ly}\alpha$ or CIV , the color of the arc is inconsistent with this interpretation. The Lyman limit in that case would fall in the middle of the B-band, and the arc would be much redder than the $B_J\text{-}R \sim 1.1$ value observed by Fischer and Tyson (1997).

The emission line is fully consistent with the line being the [OII] line. In that case, however, the H β and [OIII] line emissions should be within the spectral region observed from the ground. Unfortunately, all of these lines would be hidden beneath the strong atmospheric bands which abound in this region of the spectrum. Spectra obtained with HST and STIS can provide an unambiguous determination of the redshift of the arc by detection of other emission lines. In our subsequent analysis, we will assume that the redshift of the arc is 0.8, noting that the mass estimate is not affected by more than 30% even if the redshift is as high as 4.

The southern arc is slightly fainter but its distance is only about 2% larger than the distance to the northern arc. Furthermore, its center of curvature is almost centered at the bright galaxy. A simple physical model, consistent with these data and an Einstein radius equal to the distance from the center to the arc in the lens plane, predicts that the redshift of this arc is between 0.7 and 1. The lack of an emission line detection at this wavelength suggests that either the source is a galaxy devoid of emission lines, or the emission line is hidden beneath the abundance of atmospheric lines.

6. Gravitational mass and the mass-to-light ratio

Fischer and Tyson (1997) have obtained a deep ground-based image of the cluster with a field size of dimension $(14')^2$, which they have used for a mass-modeling of the cluster (also see Tyson and Fischer, 1995). They detect a shear-signal in the background galaxies in the radial range of 35'' to 400'' from the cluster center and estimate the redshift of the arcs to be $1.4^{+1.4}_{-0.35}$ and $1.6^{+2.0}_{-0.5}$ respectively. Here we confine ourselves to the strong lensing regime ($r < 35''$). The fact that the two arcs on the opposite sides (nos. 1 and 4) have rather large magnifications and the center of the radius of curvature of the arcs lies close to the central galaxy makes the mass modeling rather straight forward. In such a case, the angular radius θ_E corresponding to the Einstein radius of the lensing galaxy R_E , can be expressed as (Schneider, Ehlers and Falco, 1992; Blandford and Narayan, 1992)

$$\theta_E^2 = \frac{4GM D}{c^2}, D = \frac{D_{ds}}{D_d D_s} \quad (1)$$

where M is the the mass of the lensing object, D_d is the the distance to the lensing object, D_{ds} is the the distance from the lens to the source, and D_s is the distance from the observer to the source (all distances being angular distances). We can assume θ_E to be the same as the distance from the lensing galaxy to the arc (34.9'' for the northern arc). Since the redshifts of the lensing galaxy and the arc are now known, we can derive the projected mass within this radius. The resulting mass is $6.3 \times 10^{14} M_\odot$ (assuming $\Omega = 1$, $\Lambda = 0$ and $H_0 = 50 \text{ km s}^{-1} \text{ Mpc}^{-1}$). To derive the total luminosity, we measured the fluxes of all (~ 100) galaxies within the radius of the assumed Einstein ring of the cluster. To derive the magnitudes in the CCD-clear aperture, we use the following formula as determined from the cycle 7 calibration programs:

$$V(\text{Johnson}) = -2.5 \log(c/s) + 25.69 + 0.479(V - I) \quad (2)$$

where c refers to counts obtained with $\text{gain}=1$. Using the magnitude and color information for the two central CD galaxies (given in Table 3) and other galaxies in the field, we estimate that the combined flux from these two galaxies is approximately 38% of the total flux from all the galaxies (assuming the contribution from even fainter galaxies is small). For the luminosity distance to the cluster, we use $H_0=50 \text{ km s}^{-1}$, and $\Lambda = 0$, which gives a distance of 2950 Mpc corresponding to a distance modulus of $(m-M) = 42.3$. Applying a K-correction of 0.6 mag appropriate for the cluster, the derived total luminosity of all the galaxies is $5 \times 10^{11} L_\odot$. This implies a mass-to-light ratio of ~ 1200 within the assumed radius of the Einstein ring.

7. Discussion

RX J1347.5-1145 is the most luminous X-ray cluster and is one of the most massive of all clusters. We have used the STIS images and the spectroscopic information of the arcs to derive a mass of $6.3 \times 10^{14} M_\odot$ within the Einstein ring (240 Kpc). The total surface mass within this region as derived from the X-ray observations is $2.1 \times 10^{14} M_\odot$ (Schindler et al. 1996) to $6.8 \times 10^{14} M_\odot$ (Allen, 1997). Thus the ratio of the gravitational mass (which we can assume to be the total mass within the radius) to X-ray mass is between 1 and 3. The surface *gas* mass within this radius, as derived from the X-ray observations, is $\sim 3.5 \times 10^{13} M_\odot$. We can assume this gas to be baryons, which imply that baryons contribute at least $\sim 6\%$ to the total mass in this central region of the cluster. Since the cluster is dominated by dark matter with mass-to-light ratio of ~ 1200 , this also implies that at least $\sim 6\%$ of the *dark matter* in this region is baryonic. It is interesting to note that Hottari et al. (1997) have recently derived a the mass-to-light ratio of ~ 3000 for a luminous X-ray cluster, where they find that the bulk of the X-ray emitting gas is also rich in metals.

From a weak-lensing model, Fischer and Tyson (1997) have derived a mass of $1.0 \times 10^{15} M_\odot$ within a spherical radius of 1 Mpc (400 arcsec). As derived from the X-ray observations, the total mass within this radius is $5.8 \times 10^{14} M_\odot$, and the total surface mass within this radius is $1.0 \times 10^{15} M_\odot$ (Schindler at al, 1996). This implies that the discrepancy between the gravitational and the X-ray mass for the whole cluster is also not large. The mass-to-light ratio, as derived from the ratio of the gravitational mass to the combined luminosity from all the galaxies within the field, is 200 for the whole cluster (Fisher and Tyson, 1997). This is similar to what is found in other large clusters such as Coma (Hughes, 1989), but lower than what is seen in the central region of RX J1347.5-1145.

In conclusion, the discrepancy between the X-ray mass and the gravitational mass is not large either in the central or outer part of the cluster. The cluster is dominated by dark matter, and the baryonic component in the central region is at least $\sim 6\%$.

We would like to thank Mike Potter for assistance with the spectral data reduction. We thank

Stella Seitz and Sabine Schindler for useful comments on the manuscript.

REFERENCES

- Allen, S.W., 1997, Preprint (astro-ph/9710217).
- Baum S. et al., 1996, STIS Instrument Handbook, Version 1.0 (Baltimore: STScI)
- Bahcall, N., 1988, *Ann. Rev. Astron. Astrophys.* **26**, 631.
- Binney, J., Tremaine, S., 1987, *Galactic Dynamics*, Princeton Univ. Press, p.213
- Blandford, R.D., Narayan, R., 1992, *Ann. Rev. Astron. Astrophys.*, **30**, 311
- Fischer, P., Tyson, J.A., 1997, *Astron. J.*, **114**, 14
- Gioia, I.M., Luppino, G.A., 1994, *ApJ Supp. Ser.*, **94**, 583
- Hattori, M., et al., 1997, *Nature*, **388**, 146
- Hughes, J.P., 1989, *APJ*, **337**, 21
- Schindler, S., Guzzo, L, Ebeling, H., Böhringer, H., Chincarini, G., Collins, C.A., De Grandi, S., Neumann, D.M., Briel, U.G., Shaver, P., Vettolani, G., 1995, *Astron. Astrophys.*, **299**, L9
- Schindler, S., Hattori, M., Böhringer, H., 1996, *Astron. Astrophys.*, **317**, 646
- Schneider, P, Ehlers, J. and Falco, E.E., 1992, *Gravitational Lensing*, Springer-Verlag
- Tyson, J.A., Fischer, P, 1995, *ApJ*, **446**, L55
- White, D.A., Fabian, A.C., 1995, *MNRAS*, **273**, 72

Table 1: Log of the ground-based spectroscopic observations

Position	Date of Observation	Grating	Integration time (sec)	Wavelength range (Å)	Resolution (Å)
Northern arc	June 28, 1995	R300	6000	6200 - 9600	8
Northern arc	June 28, 1995	B300	6000	3600 - 6800	8
Southern Arc	June 29, 1995	R300	6300	6200 - 9600	8
Southern Arc	June 29-30, 1995	B300	7200	3600 - 6800	8
2 central galaxies	June 28, 1995	R300	3600	6200 - 9600	8

Table 2: Details of the arcs as seen in the STIS images.

Arc	Length (L)* (arcsec)	Width (W)* (arcsec)	L/W	Distance from the central galaxy (arcsec)	Arc Location RA (2000)	Dec (2000)
1	5.85	0.76	7.7	34.2	13:47:32.03	–11:44:42.1
2	2.09	0.33	6.4	31.6	13:47:31.13	–11:44:38.7
3	2.87	0.33	8.8	40.2	13:47:27.89	–11:45:08.5
4	7.81	0.50	15.6	36.3	13:47:29.26	–11:45:39.3
5	1.87	0.20	9.2	46.0	13:47:31.81	–11:45:51.7

*The STIS point spread function is 0.085 arcsec FWHM for the CCD and the clear aperture.

Table 3. V Magnitudes of the galaxies and the arcs*

Filter	Eastern Galaxy	Central Galaxy	Arc 1	Arc 2	Arc 3	Arc 4	Arc 5	(V-I)
Clear	19.6	19.2	22.2	22.2	23.3	21.5	23.2	1.0 assumed
Long-pass	...	19.2 [†]	...	22.3 [‡]	0.93 [†] , 1.4 [‡]

[†]The measured color term for the brightest galaxy in the field. No color information is available for the eastern CD galaxy.

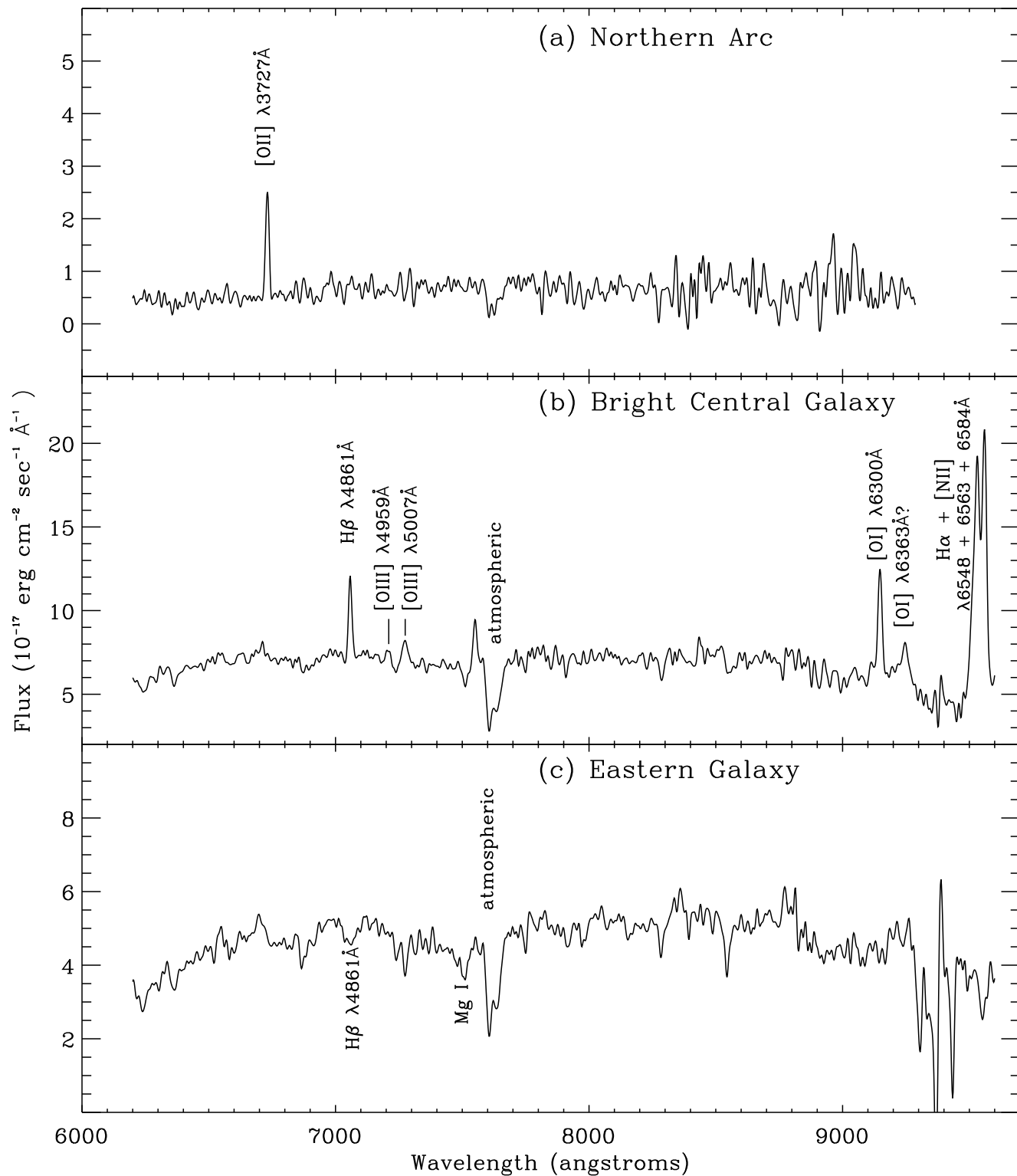
[‡]The measured color term for arc 2. This is the only arc for which color information can be measured.

*The uncertainties in the magnitudes are: 0.2 for the two galaxies, and 0.4 for the arcs.

Fig. 1.— The spectra of the northern arc and the two galaxies. The region beyond 9000 Å is heavily affected by atmospheric lines. The weak features near 9000 Å in case of the arc and the fainter galaxy are most likely due to the noise in sky subtraction. The arc shows a strong emission line at 6730 Å, the central galaxy shows many emission lines, and the eastern galaxy shows mostly absorption features.

Fig. 2.— (Plate 1) The STIS mosaic image of the cluster RX J1347.5-1145 taken with the CCD and the clear filter. The central galaxy was placed in the overlapping region of all the images to increase the S/N. The two large arcs (1 and 2) and other possible arcs are marked in the figure.

Fig. 3.— (Plate 2) An enlarged view ($6.2'' \times 6.2''$) of the central galaxy, which shows a clear jet-like structure on one side, and a similar but much fainter structure on the opposite side. These structures, which may be jets or tidal tails, are about $0.6''$ long, which corresponds to a length of ~ 3 kpc.



This figure "fig2.gif" is available in "gif" format from:

<http://arxiv.org/ps/astro-ph/9709239v2>

This figure "fig3.gif" is available in "gif" format from:

<http://arxiv.org/ps/astro-ph/9709239v2>